Available online at www.sciencedirect.com

SCIENCE DIRECT®

Journal of Volcanology and Geothermal Research 135 (2004) 29–49

Journal of volcanology and geothermal research

www.elsevier.com/locate/jvolgeores

MODVOLC: near-real-time thermal monitoring of global volcanism

Robert Wright*, Luke P. Flynn, Harold Garbeil, Andrew J.L. Harris, Eric Pilger

Hawaii Institute of Geophysics and Planetology, University of Hawaii, 1680 East-West Road, Honolulu, HI 96822, USA

Accepted 5 December 2003

Abstract

MODVOLC is a non-interactive algorithm developed at the Hawaii Institute of Geophysics and Planetology (HIGP) that uses low spatial resolution (1-km pixel-size) infrared satellite data acquired by the Moderate Resolution Imaging Spectroradiometer (MODIS) to map the global distribution of volcanic thermal anomalies in near-real-time. MODVOLC scans the Level-1B MODIS data stream, on a pixel-by-pixel basis, for evidence of pixel and sub-pixel-sized high-temperature radiators. Once a hot spot has been identified its details (location, emitted spectral radiance, time, satellite observation geometry) are written to ASCII text files and transferred via FTP to HIGP, from where the results are disseminated via the internet http://modis.higp.hawaii.edu). In this paper, we review the underlying principles upon which the algorithm is based before presenting some of the results and data that have been obtained since its inception. We show how MODVOLC reliably detects thermal anomalies at a large number of persistently and sporadically active volcanoes that encompass the full range of common eruptive styles including Erebus (Antarctica), Colima (México), Karymsky (Kamchatka), Popocatépetl (México), Etna (Italy), and Nyiragongo (Democratic Republic of Congo), amongst others. We also present a few cautionary notes regarding the limitations of the algorithm and interpretation of the data it provides.

Keywords: MODIS; MODVOLC; remote sensing; thermal monitoring

1. Introduction

The origins of satellite volcanology can be traced back as far as 1965, when data from the Nimbus I High Resolution Infrared Radiometer (HRIR) were used to demonstrate that Kilauea volcano on the Big Island of Hawaii emitted more thermal radiance than its inactive neighbour, Mauna Loa (Gawarecki et al., 1965). Subsequent work by Williams and Friedman (1970) pointed to the potential of such data for quantifying thermal emission from volcanoes, during an eruption at Surtsey, Iceland, in 1966. However, it was not until after the pioneering work of Francis and McAllister (1986), Francis and Rothery (1987) and Rothery et al. (1988) that thermal remote sensing, and in particular the Landsat Thematic Mapper (TM), became established as a tool for studying active volcanoes. Subsequent research has applied and extended the techniques they presented and the range of volcanic parameters that can be derived, with particular attention paid to the thermal analysis of active lava flows (e.g. Oppenheimer, 1991; Flynn et al.,

* Corresponding author.
E-mail address: wright@higp.hawaii.edu (R. Wright).

0377-0273/$ - see front matter © 2004 Elsevier B.V. All rights reserved.
doi:10.1016/j.jvolgeores.2003.12.008

1994; Wright et al., 2001), lava domes (Oppenheimer et al., 1993; Kaneko et al., 2002a,b), lava-lakes (Oppenheimer and Francis, 1997; Harris et al., 1999) and fumarole fields (Harris and Stevenson, 1997; Kaneko and Wooster, 1999).

Although high-spatial resolution imagery (e.g. 30- to 120-m pixels) can yield useful information regarding the detailed thermal properties of volcanic features (Donegan and Flynn, 2004-this volume, the low-temporal resolution at which they are acquired (typically once every 16 days) precludes their use for monitoring dynamic volcanic processes. For this reason, volcanologists have looked to the low-spatial- (1- to 4-km) but high-temporal- (30 min to 3 day) resolution data provided by meteorological satellites such as the Advanced Very High Resolution Radiometer (AVHRR), the Along-Track Scanning Radiometer (ATSR) and the Geostationary Operational Environmental Satellite (GOES), to fulfil this role (see Oppenheimer, 1998, for a review). AVHRR, ATSR and GOES have proven to be effective eruption monitoring tools despite of the fact that the volcanic features of interest are usually much smaller than the nominal pixel size of the instruments (1-km for AVHRR and ATSR and 4-km for GOES). This can be attributed to their ability to detect emitted radiance in the shortwave infrared (SWIR) part of the electromagnetic spectrum, a region in which active lava flows, vents and domes emit copious amounts of energy.

Initial research concentrated on demonstrating the potential of these sensors. Although volcanic thermal anomalies had been observed fortuitously in AVHRR data several times before (e.g. Weisnet and D'Aguanno, 1982; Scorer, 1986) the Alaskan Volcano Observatory (AVO) was amongst the first to actually use AVHRR to study volcanoes, during the 1989–1990 eruption of Redoubt volcano, Alaska (Schneider et al., 2000). AVHRR acquires data at a nominal spatial resolution of 1 km, twice per day (although a higher data frequency is possible when more than one AVHRR is in orbit, or at high latitudes where adjacent swaths overlap). Subsequent work by Harris et al. (1997a,b) showed how AVHRR could be used to provide high-temporal resolution chronologies of large effusive basaltic eruptions and persistent activity at a range of volcanoes including Etna (Sicily), Erebus (Antarctica), and Krafla (Iceland).

Despite having a lower temporal resolution than AVHRR (an average revisit period of 3 days), Wooster and Rothery (1997a,b) demonstrated how useful time-series of volcanic thermal activity at Làscar (Chile) and Fernandina (Galapagos Islands) could also be compiled using ATSR data. GOES data had previously been used extensively for monitoring biomass burning (e.g. Prins and Menzel, 1994), before Harris et al. (1997c) showed how even at a pixel size of 4 km, effusive volcanic eruptions could be monitored with a temporal resolution of 15–30 min when they used infrared data from the geostationary GOES satellite to document the development of the episode 54 eruption of Kilauea volcano, Hawaii.

These studies involved the use of high-temporal resolution data for retrospective documentation of eruptive events. However, the techniques they develop therein provided the basis and impetus for the next logical step; the incorporation of meteorological satellite data into operational volcano monitoring systems. The AVO were the first to use AVHRR in a real-time monitoring capacity when, during the 1992 eruption of Mount Spurr, images were downloaded, calibrated, and ready for analysis within five minutes of satellite overpass (Schneider et al., 2000). The AVO currently uses AVHRR to monitor more than 100 potentially active volcanoes of Alaska and the Kamchatka Peninsula. A proto-type AVHRR-based system is also being developed to monitor volcanic activity in Japan (Kaneko et al., 2002a,b).

Following on from the work of Harris et al. (1997c), researchers at the Hawaii Institute of Geophysics and Planetology (HIGP) developed a system that uses direct-broadcast GOES data to monitor thermal activity at a wide range of volcanoes in the Pacific Ocean, South and Central America, and the continental USA (see Harris et al., 2001 for a full description of the system and web site). This system not only provides greater spatial coverage than that of the AVO but, significantly, makes the results of the analysis freely available via the internet http://goes.higp.hawaii.edu), usually within 15 min of image acquisition.

Although AVHRR and GOES have been used for some years to monitor active volcanism, neither sensor has been integrated into a fully global monitoring system. The AVO AVHRR-based system monitors volcanism solely in the North Pacific while the

scope of the HIGP GOES system is confined to the Pacific and its surrounding 'Ring of Fire'. This paper describes how data from the moderate resolution imaging spectro-radiometer (MODIS), launched in 1999 on-board NASA's first Earth Observing System (EOS) platform, Terra, have been used as the basis for a new global thermal monitoring system. This system, MODVOLC, is the first to monitor thermal activity at all of the Earth's sub-aerial volcanoes and make the results available via the internet in near-real-time.

2. Infrared volcano monitoring and the MODIS sensor

The principles of infrared volcano monitoring have been reviewed many times before (see Rothery et al., 1995). In essence, hot-spot detection using low-spatial resolution satellite data relies on the fact that the presence of material at magmatic temperatures (e.g. ~ 200–1100 °C) within an otherwise thermally homogenous pixel causes the amount of spectral radiance emitted in the SWIR to increase dramatically relative to that in the long-wave infrared part of the electromagnetic spectrum. Fig. 1 illustrates this principle using data acquired by ATSR during a recent summit eruption of Mount Etna. Here, emitted spectral radiance at 4 and 12 μm is displayed for each 1-km pixel as a percentage of the lowest value recorded within the 6 × 6 pixel box. The presence of high-temperature material within Etna's summit craters causes the radiance emitted at 4 μm to increase by as much as 800% above the levels recorded for pixels located away from the summit craters, compared with less than 5% at 12 μm. Clearly, SWIR data are a very effective means for detecting the presence of pixel- or sub-pixel-size lava bodies.

Fig. 2 shows a nighttime MODIS band 22 (3.929–3.989 μm) sub-scene of the island of Montserrat. MODVOLC was initially designed to use only nighttime data, as the occurrence of solar reflection in daytime imagery masks thermal emission at 4 μm, making volcanic hot spots harder to detect. A daytime version of the algorithm has been developed and implemented on a preliminary basis, although a full evaluation of its operational performance has yet to be conducted. As a result, this paper discusses only the development, testing and results obtained from the nighttime version of the MODVOLC algorithm. Here, high levels of emitted radiance at 4 μm results in bright pixel tones on images such as the one shown in Fig. 2. The white pixels in the southeast quadrant of the island correspond to high-temperature pyroclastic flows emplaced on and around the day of image acquisition and are easily distinguishable from other pixels in the image.

MODIS was launched into a sun-synchronous orbit on-board NASA's first EOS platform, Terra, in December 1999. MODIS nominally acquires data once by day and once by night in each 24-h period, although this varies as a function of latitude. Whereas at high latitudes adjacent swaths overlap significantly and temporal resolution improves, at low latitudes gaps occur between adjacent imaging swaths. As a result, complete global coverage is achieved every 2 days.

In common with AVHRR and GOES, MODIS acquires data in the important 4 and 11–12 μm wavelength regions. It does, however, offer significant advantages over both of these sensors. Whereas AVHRR and GOES possess only three wavebands

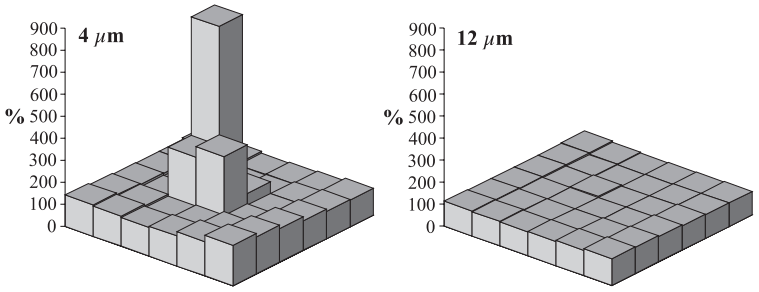

Fig. 1. ATSR radiance maps of the summit region of Mount Etna, recorded on 17 March 1998. For each wavelength, pixel radiance is expressed as a percentage of the lowest radiance recorded in the 6 × 6 pixel kernel.

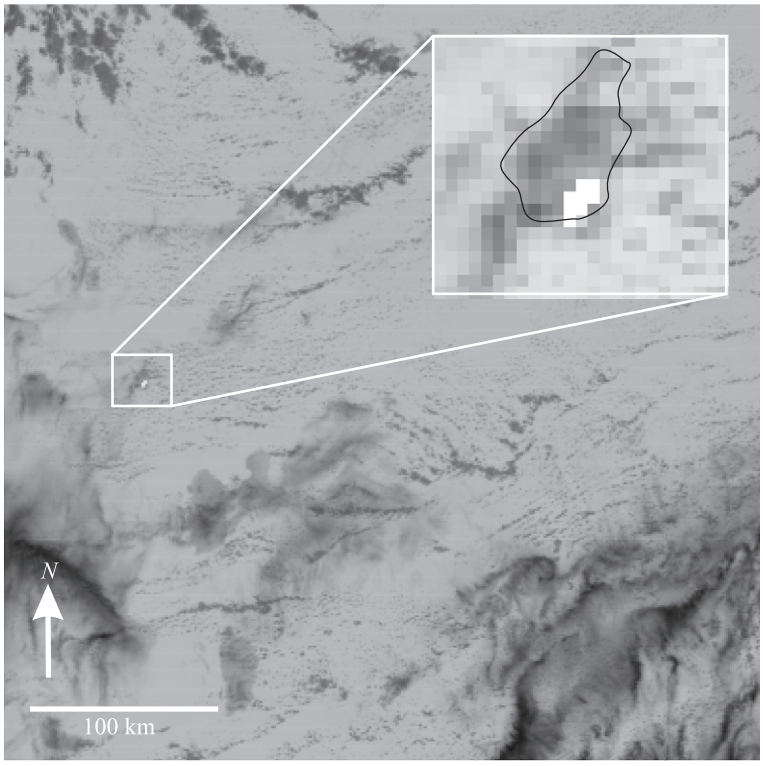

Fig. 2. Nighttime MODIS band 22 (3.959 μm) image of Montserrat, Lesser Antilles. Main image is a 400-km^2 sub-set of the original, and has been rotated 180° to place north at the top. Inset image shows the island of Montserrat. Bright pixels in the southeastern part of the island are volcanic hot spots associated with the enduring lava dome eruption at Soufriere Hills volcano.

suitable for hot-spot detection, MODIS provides up to 10, of which three are used by the MODVOLC algorithm we describe here: bands 21, 22, and 32. Bands 21 and 22 both detect emitted radiance in the 3.929–3.989-μm interval at a spatial resolution of 1 km, with a radiometric accuracy (expressed as noise equivalent temperature variation; NEΔT) of 2.0 and 0.07 K, respectively. Importantly, while band 22 has a saturation temperature of ~ 330 K (similar to the 4-μm channels provided by AVHRR and GOES), band 21 was designed to have a much higher saturation temperature of ~ 500 K (Kaufman et al., 1998). This is a welcome improvement, given the ease with which AVHRR and GOES 4-μm channels saturate over high-temperature targets. Band 32 (11.770–12.270 μm; NEΔT = 0.05 K; spatial resolution = 1 km) also has a higher saturation temperature than its counterparts on AVHRR and GOES, measuring up to 420 K.

3. The MODVOLC algorithm and web site

Wright et al. (2002a) provide a full description of how the MODVOLC algorithm was developed, tested

Fig. 3. (a) Planck curves calculated for thermally homogenous surfaces at 3.959 and 12.02 μm. The 3.959–12.02-μm difference is plotted on the right-hand ordinate. (b) Planck curves for a range of blackbody surfaces. Curves for thermally homogenous surfaces exhibit an increasing slope between 4 and 12 μm over the range of temperatures presented. However, this relationship breaks down for pixels containing sub-pixel-sized radiators, as the amount of radiance emitted at 4 μm increases dramatically when compared to that at 12 μm. As a result, hot-spot pixels can exhibit similar slopes to cold, thermally homogenous pixels. (c) Contrast-enhanced MODIS band 22 image of the Big Island of Hawaii, acquired on the night of 2 February 2001. The image has been rotated 180°. Main image measures ~ 2354 × 1354 km. Active lava flows associated with the ongoing eruption at Kilauea volcano are obvious as a group of bright pixels in the second inset image. (d) MODIS band 22[21]–32 values calculated for several different cover types present in (c). (e) NTI values calculated for the pixels depicted in (d).

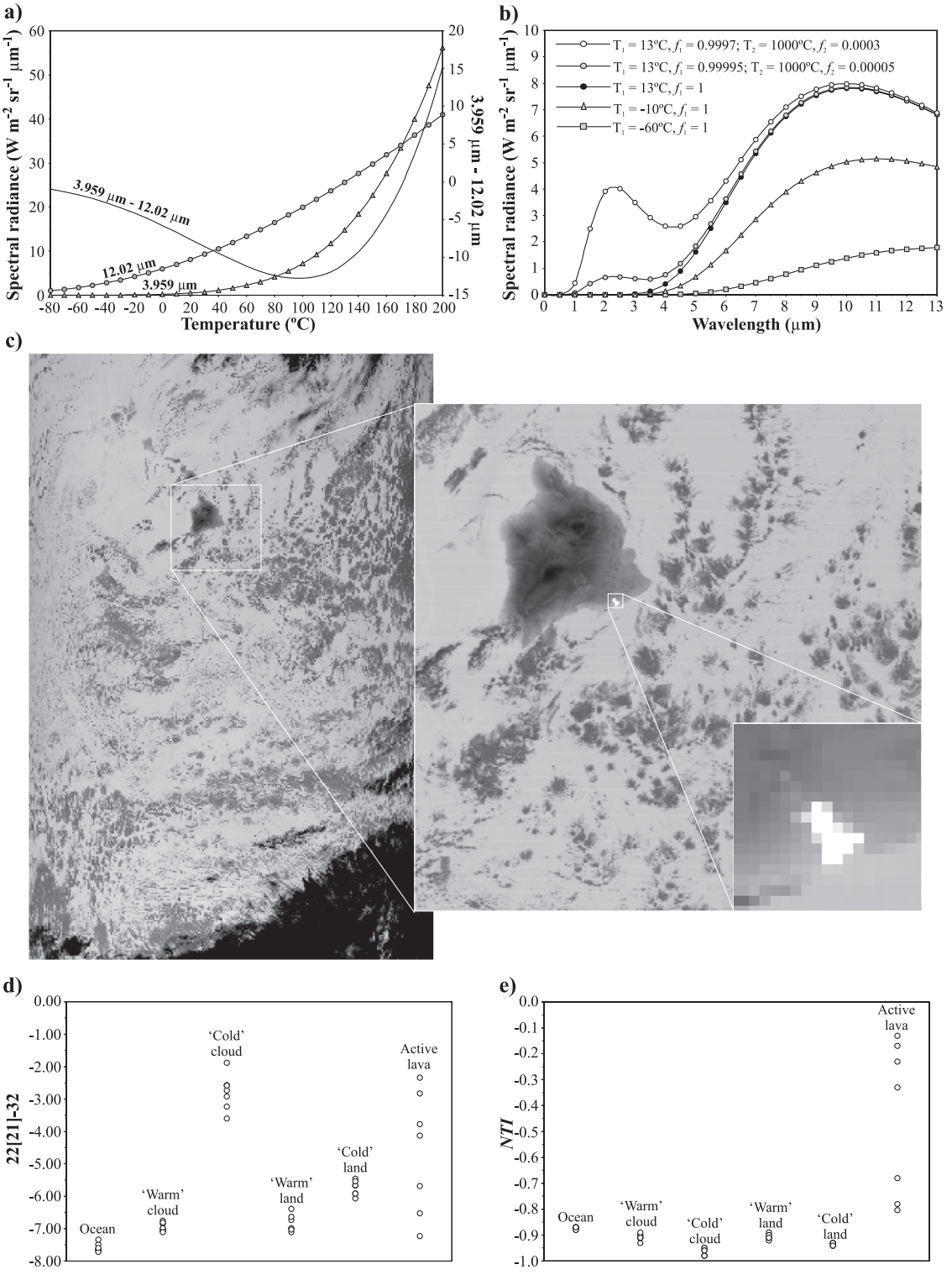
a)
Spectral radiance (W m-2 sr-1 μm-1)
3.959 μm - 12.02 μm
12.02 μm
3.959 μm
3.959 μm - 12.02 μm
Temperature (ºC)
b)
T1 = 13ºC, f1 = 0.9997; T2 = 1000ºC, f2 = 0.0003
T1 = 13ºC, f1 = 0.99995; T2 = 1000ºC, f2 = 0.00005
T1 = 13ºC, f1 = 1
T1 = -10ºC, f1 = 1
T1 = -60ºC, f1 = 1
Spectral radiance (W m-2 sr-1 μm-1)
Wavelength (μm)
c)
d)
22|21|-32
Ocean
'Warm' cloud
'Cold' cloud
'Warm' land
'Cold' land
Active lava
e)
NTI
Ocean
'Warm' cloud
'Cold' cloud
'Warm' land
'Cold' land
Active lava

and implemented. Here, we discuss the main aspects of the system. Although human identification of hot spots in 4-μm satellite data is easy (Fig. 2), visual inspection is impractical as a basis for monitoring global volcanism in near-real-time due to the volume of data. Instead, non-interactive hot-spot monitoring using low-spatial resolution satellite data has historically been achieved using a combination of two techniques: the spectral comparison method (e.g. Prins and Menzel, 1992) and the spatial comparison method (e.g. Flasse and Ceccato, 1996). The MODIS Fire Products (see Justice et al., 2002) exploit both of these methods to detect wildfires and other biomass burning events. However, operational constraints imposed by the Goddard Space Flight Center (GSFC) Distributed Active Archive Center (DAAC) on the MODIS volcano product, which was always envisaged as running early in the MODIS Level 1B processing chain with no other data dependencies, meant that neither of these approaches could be utilised in the development of MODVOLC (Flynn et al., 2002). Restrictions on the number of mathematical operations that MODVOLC could utilise prevented the calculation of pixel brightness temperature (thus, prohibiting the spectral comparison method) while the requirement that MODVOLC should be a point operation precluded the use of the spatial comparison approach (which relies of contextual analysis of a pixel and its neighbourhood of pixels). Given these and other constraints (i.e. limits on the number of wavebands employed, inability to store image data), we developed a new method for non-interactively discriminating hot spots in MODIS data. The MODVOLC algorithm is a point operation which analyses the Level 1B MODIS radiance data from three wavebands (21, 22, and 32) using four mathematical operations.

Surfaces that are thermally homogenous at the pixel scale can be discriminated on the basis of differences in the amount of radiance they emit at 4 and 12 μm (Fig. 3a). However, this helps little in discriminating sub-pixel-sized volcanic hot spots, a consequence, ironically, of the contrasting nature of the relationship between temperature and emitted radiance at 4 and 12 μm lauded in Section 2. Fig. 3b shows a series of Planck curves for a range of thermally homogenous and inhomogenous surfaces, representative of those recorded in the nighttime MODIS image of the state of Hawaii illustrated in Fig. 3c. The slope of the curves between 4 and 12 μm (MODIS bands 22 or 21 and 32, respectively) increases as the temperature of the thermally homogenous surfaces increases, allowing land at ~ 13 °C to be discriminated from clouds at ~ -10 °C using a simple 4–12 μm (band 22 [or 21]–32) operation (Fig. 3d). However, this simple differencing approach fails to distinguish active lava flows, which show a large degree of overlap with other cover types in the Hawaii data set. This is because the addition of a small high-temperature volcanic radiator to an otherwise thermally homogenous pixel causes the slope of the combined Planck curves to decrease, because emission at 4 μm increases dramatically relative to that at 12 μm (Section 2). Furthermore, relatively small changes in the fractional area of the volcanic heat source cause large variations in emitted 4-μm radiance (Fig. 3b), so a pixel containing such a feature can exhibit a wide range of 4–12-μm difference values.

However, by normalising the difference between the recorded 4- and 12-μm radiance by the sum of the 4- and 12-μm radiances, an index can be obtained that is weighted to those surfaces that emit substantial levels of radiance at 4 μm (i.e. the lava flows) rather than those which emit lower amounts of radiance at this wavelength (i.e. the cold clouds). This is the basis of our Normalised Thermal Index (NTI), which satisfies all of the operational criteria imposed by the GSFC DAAC, and allows MODIS pixels containing active lava flows to be effectively discriminated (Fig. 3e) from all other pixels within the Hawaii image. NTI is computed using:

$$\mathrm{NTI} = \frac{22 - 32}{22 + 32}, \tag{1}$$

or (when band 22 is saturated):

$$\mathrm{NTI} = \frac{21 - 32}{21 + 32}, \tag{2}$$

where 21, 22, and 32 refer to the amount of spectral radiance (W m^{-2} sr^{-1} μm^{-1}) in MODIS bands 21, 22, and 32, respectively.

Fig. 3e indicates that an NTI threshold of -0.82 would effectively distinguish active lava pixels in the Hawaii data set depicted in Fig. 3c. This is further illustrated in Fig. 4a, which shows the histogram of

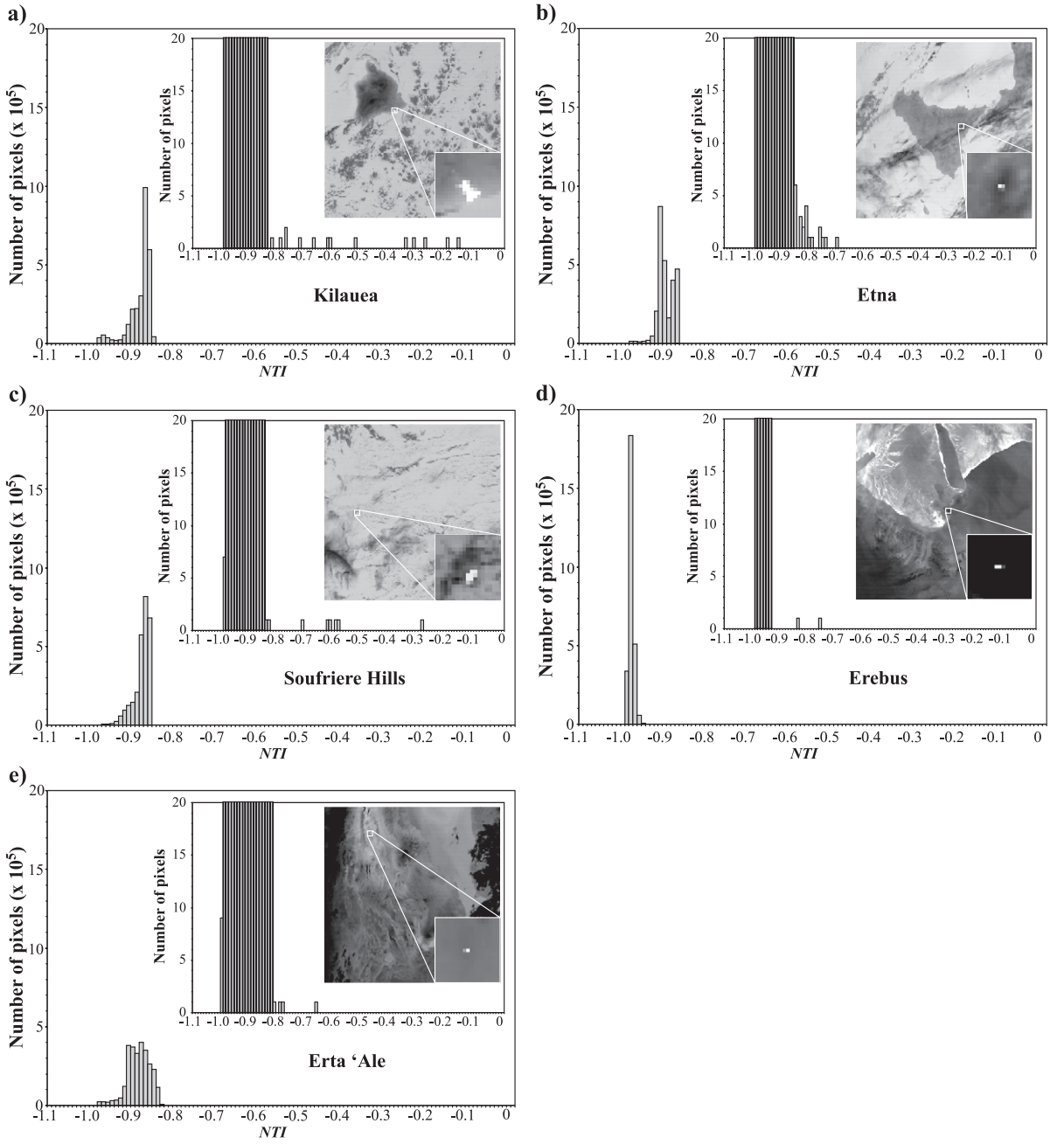

Fig. 4. NTI histograms of all 2,748,620 pixels contained within MODIS scenes of (a) Kilauea volcano (acquired on 2 February 2001), (b) Mount Etna (acquired on 8 November 2000), (c) Soufriere Hills volcano (acquired on 23 February 2001), (d) Mount Erebus (acquired on 1 May 2001), and (e) Erta 'Ale (acquired on 13 November 2000). In each case, the right-hand tail of the distribution (visible only in the insets, which have a magnified vertical scale) is composed solely of hot-spot pixels.

NTI values calculated for every pixel in this image. Hot-spot pixels form a very distinctive tail to the NTI distribution. Fig. 4b to e shows similar histograms calculated from nighttime MODIS images of Etna (Sicily), Soufriere Hills volcano, (Montserrat), Erebus (Antarctica) and Erta 'Ale (Ethiopia), respectively, which all exhibit the same characteristic hot-spot tail. It is apparent however that a single NTI threshold value will not successfully isolate all hot-spot pixels at all of these volcanoes. This is because the 4- and 12-μm radiances from which the NTI is calculated are not merely a function of the size and temperature of the hot spot, but also the temperature of the ambient surfaces surrounding the hot spot. Unfortunately, MODVOLC has to rely upon a single globally and seasonally applicable NTI threshold value, given that the algorithm must run with no other data dependencies (Flynn et al., 2002).

Fig. 4 illustrates this problem. An NTI threshold of −0.82 would result in accurate identification of 14 hot-spot pixels in the MODIS Hawaii data set. The same threshold would also successfully identify one hot spot in the Mount Erebus data set. However, to identify both hot spots associated with Erebus' lava-lake (Fig. 4e, inset) would require a lower NTI threshold of −0.84. However, such a threshold would result in more than 100,000 false alerts (Fig. 4d) at Erta 'Ale volcano, where ambient surface temperature are much higher than those in the Antarctic. A threshold of −0.84 would result in 44 alerts in the Hawaii data set, visual inspection of the MODIS imagery indicates than 23 of these would be false. The problem is essentially one of setting the NTI threshold low enough that MODVOLC identifies as many real hot-spots as possible, whilst not encroaching onto the main body of the histograms displayed in Fig. 4, as this would result in large numbers of false positives. In order to achieve this, we analysed NTI histograms for more than 100 MODIS data sets covering a wide range of geographic locations, to empirically determine an NTI threshold that would be stable both globally and seasonally. For the MODIS scenes, we analysed an NTI threshold of −0.80 resulted in reliable detection of volcanic hot spots without returning a single false positive.

Fig. 5 shows how the MODVOLC algorithm operates. The algorithm interrogates each MODIS Level 1B data set on a pixel-by-pixel basis. Although

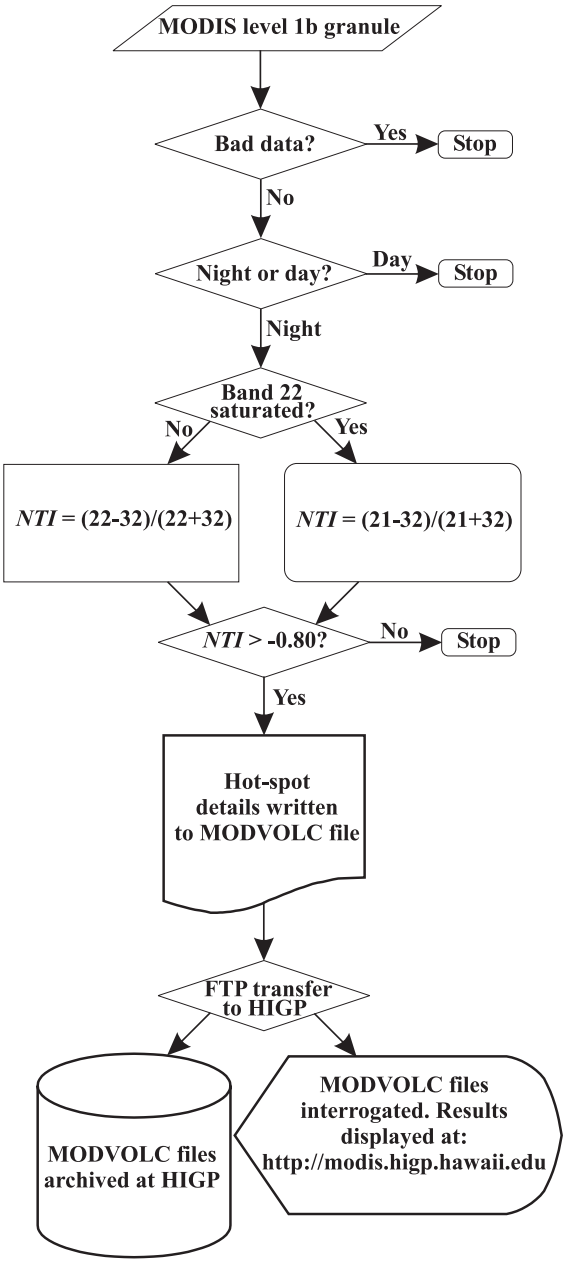

Fig. 5. Flow diagram illustrating the operation of the MODVOLC nighttime algorithm.

MODIS is a 12-bit instrument (i.e. 4096 discrete measurement levels), the raw instrument response is re-scaled to a 16-bit unsigned (i.e. 0–65535) scaled integer (SI) representation for storage. The lower half

of this range (i.e. 0–32767) is used for storing science data, which is converted to standard radiance units (W m^{-2} sr^{-1} μm^{-1}) using calibration parameters stored within each MODIS hierarchical data format (hdf) granule. SIs in excess of this cut-off are used to indicate various types of bad data, and are termed 'reserve values'.

Pixels are categorised as nighttime or daytime on the basis of solar zenith angle (recorded for each pixel and stored in the .hdf file.) This sorting procedure was included in preparation for a daytime version of the algorithm, which we do not discuss here. The algorithm then checks whether the pixel is saturated in band 22 (saturated pixels are identified by an SI of 65533). If not, the NTI is calculated using Eq. (1). We use band 22 as our primary hot-spot detection band because of its higher radiometric precision when compared to band 21. However, if band 22 is saturated, the NTI is calculated using the low-gain channel, band 21, using Eq. (2). The resultant NTI is compared against the empirically determined threshold value of −0.80. Pixels whose NTI exceeds −0.80 are flagged as hot spots, and their details written to an ASCII text file given the GSFC Earth Science Data Type name "MODVOLC". For each hotspot, the MODVOLC file reports the time it was observed (year/month/day/hour/minute), its geodetic location (latitude/longitude in decimal degrees), emitted spectral radiance in MODIS bands 21, 22, 6, 31, and 32 (W m^{-2} sr^{-1} μm^{-1}), and satellite zenith, solar zenith and solar azimuth (all in degrees).

These MODVOLC files are then transferred via file transfer protocol (FTP) to HIGP, University of Hawaii, where the results are displayed on the internet at the following URL http://modis.higp.hawaii.edu). The appearance and functionality of the web site are subject to change, hopefully, for the better. At present, the welcome screen presents information about how the algorithm works and links to relevant publications and information contacts. From here, a hyperlink takes the user to the data themselves and a global view of all hot spots detected within the previous 24-h period. The globe is divided into a hierarchy of regions (e.g. South East Asia), sub-regions (e.g. Philippines), and target areas (e.g. Mayon), of increasing scale, accessible via hyper-link. Each page contains a link to the MODVOLC files used to generate that page ('Text alert file'), allowing the user direct access to the details of all the hot-spots portrayed. The web interface also allows access to data for any previous day or month during the period that MODVOLC has been operational (September 2000 to present).

4. Overview of results

MODVOLC detected hot spots associated with a wide range of eruptive styles at least 50 volcanoes worldwide (Table 1) between October 2000 and December 2003. This section is intended to précis some of these results within the context of the style of volcanism involved.

4.1. Lava lakes

Persistently active lava lakes are known to have existed at both Mount Erebus (Antarctica) and Erta 'Ale (Ethiopia) for at least 200 years. It is, therefore, no surprise that MODVOLC detects the presence of hot spots at these two sites on a regular basis (33% and 40% of the total number of days during our monitoring period, respectively). Fig. 6 shows hot-spot maps taken from the MODVOLC web site for each of these volcanoes. Although the algorithm we describe is very effective at identifying hot spots, it is not sophisticated enough to automatically distinguish between different types of hot spot. Thus, lava flows, vegetation fires, and industrial heat sources are not discriminated. The ability to determine the geographic location of the hot spots accurately therefore plays an important role in resolving their nature. Table 2 describes how the location of hot spots recorded at several volcanoes varied during 2002. In each case, the mean displacement of the hot spots from the published summit of the volcano (Simkin and Siebert, 1994) is given (in km), along with the standard deviation from the mean. For volcanoes with summit-crater-confined heat sources (e.g. Popocatépetl, Fuego, Erebus) MODVOLC reports hot-spot locations that are within 1 km of the expected position. At volcanoes such as Etna, Piton de la Fournaise and Kilauea, where active lava often flows unconfined in areas far removed from the summit region, both the mean and standard deviations are correspondingly higher. Similar situations arise at Shiveluch, and at Santa Maria where the currently active Caliente vent

Table 1
Volcanoes that have been identified as being thermally active by MODVOLC, and the number of separate days on which thermal emission has been detected (# alerts), for the periods 1 October 2000 to 30 November 2000, and 1 February 2001 to 31 May 2003

Volcano name (location)	Latitude/longitude	# Alerts	Type of activity
Ambrym (Vanuatu)	16.25°S, 168.12°E	95	Lava-lakes
Anatahan (Marianas Islands)	16.35°N, 145.67°E	10	Explosive eruption
Arenal (Costa Rica)	10.46°N, 84.70°W	12	Vent activity, lava flows
Bagana (Papua New Guinea)	6.14°S, 155.19°E	73	Lava dome
Bezymianny (Russia)	55.98°N, 160.59°E	21	Lava dome, pyroclastic flow
Big Ben (Heard Island)	53.10°S, 73.51°E	5	Vent activity, lava flows
Bromo (Java)	7.94°S, 112.95°E	1	Vent activity
Cleveland (Aleutian Islands)	52.82°N, 169.95°W	3	Lava flows
Colima (México)	19.51°N, 103.62°W	82	Lava dome
Dukono (Halmahera)	1.68°N, 127.88°E	11	Vent activity
Erebus (Antarctica)	77.53°S, 167.17°E	352	Lava-lake
Erta 'Ale (Ethiopia)	13.60°N, 40.67°E	399	Lava-lake
Etna (Sicily)	37.73°N, 15.00°E	176	Vent activity, lava flows
Fuego (Guatemala)	14.47°N, 90.88°W	107	Vent activity
Ibu (Halmahera)	1.48°N, 127.63°E	14	Vent activity
Karangetang (Siau Islands)	2.47°N, 125.29°E	39	Lava dome
Karymsky (Russia)	54.05°N, 159.43°E	132	Vent activity
Kavachi (Solomon Islands)	9.02°S, 157.95°E	4	Submarine
Kilauea (Hawaii)	19.42°N, 155.29°W	558	Lava flows
Kliuchevskoi (Russia)	56.06°N, 160.64°E	5	Vent activity, lava flows
Krakatau (Sunda Strait)	6.10°S, 105.42°E	10	Vent activity
Langila (Papua New Guinea)	5.53°S, 148.42°E	12	Vent activity, lava flows
Láscar (Chile)	23.37°S, 67.73°W	21	Lava dome
Lewotobi (Lesser Sunda Islands)	8.53°S, 122.78°E	2	Vent activity
Lopevi (Vanuatu)	16.50°S, 168.34°E	3	Lava flows
Manam (Papua New Guinea)	4.10°S, 145.06°E	5	Vent activity
Mayon (Philippines)	13.25°N, 123.68°E	10	Lava dome
Merapi (Java)	07.54°S, 110.44°E	73	Lava dome, pyroclastic flow
Michael (Saunders Island)	57.78°S, 26.45°W	17	Lava lake, vent activity
Miyake-jima (Japan)	34.08°N, 139.53°E	6	Vent activity
Mount Belinda (Montagu Island)	58.43°S, 26.35°W	49	*
Nyamuragira (Zaire)	1.40°S, 29.20°E	57	Lava flows
Nyirangongo (Zaire)	1.52°S, 29.25°E	66	Lava flows, lava lake
Pacaya (Guatemala)	14.38°N, 90.60°W	2	Vent activity
Pago (Papua New Guinea)	5.58°S, 150.52°E	56	Lava flows
Peuet Sague (Sumatra)	4.92°N, 96.33°E	1	Vent activity
Piton de la Fournaise (Réunion Island)	21.23°S, 55.71°E	51	Lava flows
Popocatépetl (México)	19.02°N, 98.62°W	126	Lava dome
Rabaul (Papua New Guinea)	4.27°S, 152.20°E	8	Vent activity
Reventador (Ecuador)	0.08°S, 77.66°W	5	Lava flows
Santa Maria (Guatemala)	14.75°N 91.55°W	172	Lava dome, block lava flow
Semeru (Java)	8.11°S, 112.92°E	166	Vent activity
Shiveluch (Russia)	56.65°N, 161.36°E	323	Lava dome, pyroclastic flow
Soputan (Sulawesi)	1.11°N, 124.73°E	2	Vent activity
Soufriere Hills Volcano (Montserrat)	16.72°N, 62.18°W	164	Lava dome, pyroclastic flow
Stromboli (Italy)	38.79°N, 15.21°E	98	Vent activity/lava flows
Suwanose-Jima (Japan)	29.64°N, 129.72°E	2	Vent activity
Tinakula (Santa Cruz Island)	10.38°S, 165.80°E	3	Vent activity, lava flows
Tofua (Tonga)	19.75°S, 175.07°W	1	Caldera
Tungurahua (Ecuador)	1.47°S, 78.44°W	9	Vent activity

Table 1 (*continued*)

Volcano name (location)	Latitude/longitude	# Alerts	Type of activity
Ulawun (Papua New Guinea)	5.04°S, 151.34°E	3	Lava flows
Villarrica (Chile)	39.42°S, 71.93°W	6	Lava-lake
Yasur (Vanuatu)	19.52°S, 169.43°E	51	Vent activity

* The nature of activity at Mount Belinda on Montagu Island (South Sandwich Islands) is unknown as there is no record of Holocene activity at this volcano.

is displaced some two to three km from the actual summit of Santa Maria itself.

However, standard deviations of between 0.29 and 1.44 km for volcanoes known to have relatively static heat sources do reveal a certain imprecision in the MODVOLC reported hot-spot locations. This imprecision can be attributed to various sources. Geolocation of MODIS data is achieved using the MODIS Geolocation Product (GSFC Earth Science Data Type name: MOD03), a complimentary data set that contains the geodetic coordinates for the centre point of each pixel with the corresponding Level 1B MODIS image. When MODVOLC identifies a hotspot in an image it looks to the corresponding MOD03 file to retrieve the location of that pixel. Pixel latitudes and longitudes contained within the MOD03 files are referenced to the World Geodetic System 84 (WGS-84) ellipsoid. The United States Geological Survey GTOPO30 global digital elevation model (DEM) is then used to account for terrain-induced parallax effects. GTOPO30 is a 30 arcsec DEM with a nominal spatial resolution of 1 km and an estimated vertical accuracy of 70 m.

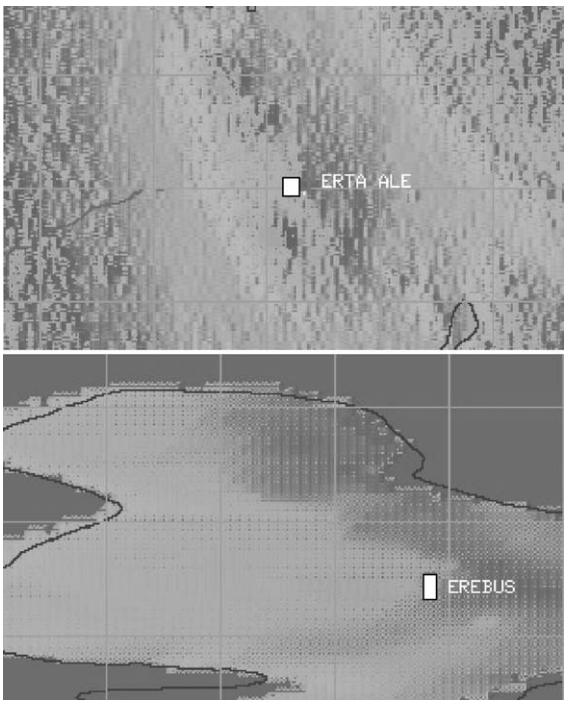

Fig. 6. Image maps taken from the HIGP MODVOLC web site (http://modis.higp.hawaii.edu) of Erta 'Ale, Ethiopia (a) and Mount Erebus, Antarctica (b), showing hot spots detected on 4 July 2001 and 19 February 2001, respectively. To aid discrimination, the hot spots in these images have a white box superimposed upon them. On the web site, hot-spots are displayed in colour, with a progression from green to yellow-red indicating increasing intensity of emitted radiance at 3.959 μm. Tick boxes measure 0.2 decimal degrees in both latitude and longitude.

As the MOD03 geolocation files report the geodetic coordinates of the *centre point* of each MODIS pixel, the location of hot spots not centred directly in a pixel will be in error by as much be as much as 50% of pixel size. This problem can become compounded if volca-

Table 2
The location of hot spots detected by the MODVOLC algorithm during 2002 for several volcanoes

Volcano	# Alerts	Mean displacement (km)	Standard deviation
Popocatépetl	46	0.65	0.29
Santa Maria	97	3.25	0.42
Colima	126	0.64	0.92
Karymsky	215	0.81	0.42
Erebus	671	0.56	0.26
Soufriere Hills	164	1.38	0.72
Fuego	246	1.15	1.44
Erta 'Ale	461	1.05	0.60
Kilauea	2394	4.47	2.06
Piton de la Fournaise	184	6.11	2.15
Shiveluch	472	3.75	0.65
Etna	600	2.94	2.93

Alerts is the total number of alerted pixels detected during this period. Mean displacement is the difference (in km) between the average location of these hotspots and the location of the summit of the volcano, as given by Simkin and Siebert (1994).

noes are imaged at high-scan angles away from the satellite nadir. Although MODIS pixels are nominally 1 km, pixel size increases with distance from nadir and at the edges of the MODIS swath (where the scan angle reaches $\pm 55°$) MODIS pixels measure ~ 2.08 km in the along-track, and ~ 4.83 km in the across-track direction. Inaccuracies in the DEM and uncertainty in the attitude of the Terra spacecraft will also have an effect. We note however, that the data presented in Table 1 indicate geolocation accuracies of ~ 1 km for the volcanoes listed. A detailed study of MODVOLC thermal alert locations conducted by Rothery et al. (2003) of industrial and agricultural fires in the United Kingdom indicated that close to sea level, accuracy can be expected to be even higher.

If remote sensing data are to be used as a proxy for prevailing levels of volcanic activity, users must be aware that individual satellite observations of emitted radiance may not be representative of long-term trends. Clearly, the coincidence of a single satellite overpass with, for example, a large lake overturning episode, would give an anomalous impression of high levels of activity. Fig. 7 shows radiance time-series produced for Erta 'Ale and Mount Erebus for the period 1 January 2001 to 31 December 2002, using the hot spots reported by MODVOLC. At both volcanoes, short-term fluctuations in radiant emission are superimposed upon a relatively stable radiance baseline. These examples are intended to illustrate how the non-interactive monitoring conducted by MODVOLC allows extended radiance time-series to be compiled with relative ease. Compiling similar radiance time-series at these and other volcanoes will allow characteristic levels of thermal activity to be determined by providing a radiance baseline against which future radiance observations can be judged.

4.2. Lava flows

Lava flows provide a relatively easy target for MODVOLC to detect (Fig. 8) as a result of both their spatial extent and radiative properties. On contact with air at ambient temperature, molten lava cools and begins to encase itself in a relatively cool crust. However, flow motion fractures this relatively cool outer crust causing material from the molten core, which is still close to the eruption temperature, to be exposed at the surface (Kilburn et al., 1995). As a result, active lava flows emit substantial amounts of SWIR radiance while they are moving (Wright et al., 2001), making them relatively easy to detect.

The January 2002 eruption of Nyiragongo (Democratic Republic of Congo) resulted in the displacement of approximately 250,000 people as lava flows encroached into the capital city of Goma and surrounding villages on the Rwandan border (United Nations Office for the Coordination of Humanitarian Affairs estimate; GVN, 2001a). The eruption is thought to have begun between 05:00 and 09:30 (local time) on 17 January 2002, and lava flows were detected by MOD-

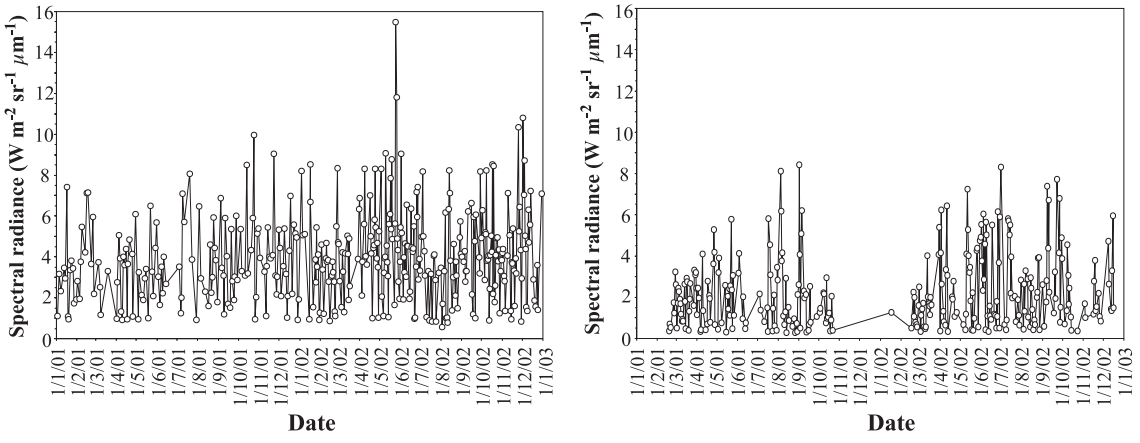

Fig. 7. Variations in the total amount of 4-μm spectral radiance detected by MODVOLC (i.e. summed for all pixels identified as hot spots by the algorithm) for the period 1 January 2001 to 31 December 2002 at Erta 'Ale (a) and Erebus (b) volcanoes.

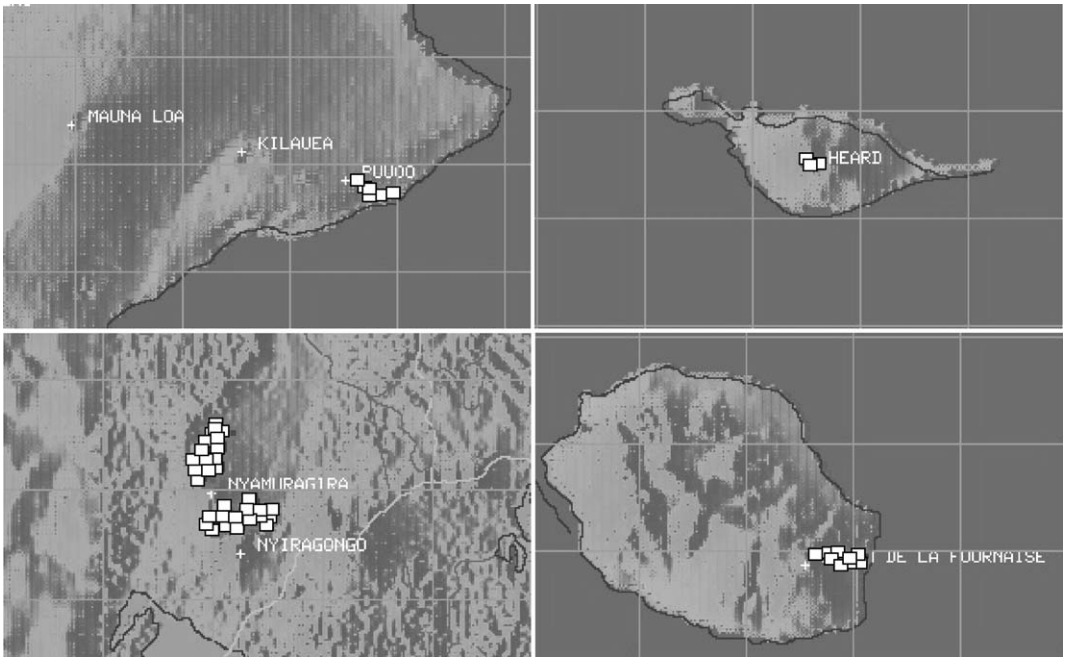

Fig. 8. Image maps taken from the HIGP MODVOLC web site showing lava flows detected at (top to bottom, left to right) Kilauea, Hawaii (2 September 2001), Big Ben volcano, Heard Island (14 February 2001), Piton de la Fournaise, Réunion Island (14 January 2002) and Nyamuragira, Democratic Republic of Congo (14 February 2001).

VOLC the following morning. The distribution of hot spots reported by MODVOLC (Fig. 9a) confirms just how spatially extensive the flows, which extended in a south–south-westerly direction and intersecting Goma before entering Lake Kivu to the south, had become at this time. The eruption was relatively short-lived, and by 21 January the initially rapid advance of lava had subsided to a situation in which only sluggish, isolated flows were observed, building up the newly formed lava delta at the edge of Lake Kivu (GVN, 2001a). This sharp decline in activity is consistent with the relatively sparse occurrence of hot spots recorded by MODVOLC on this day (Fig. 9b).

At only 4 days, this eruption is too short to pose a useful demonstration of MODVOLC as a tool for documenting the evolution of discrete eruptive events. The 2001 flank eruption of Mount Etna, however, provides a more useful test case. Fig. 10 shows how the total amount of 4-μm radiance detected by MODVOLC varied during the course of the eruption. The eruption itself, the first major flank episode at Etna since the 1991 to 1993 eruption, began on 17 July 2001 following a period of sustained summit crater activity stretching back to July 1995. Activity was concentrated along a series of fissures intersecting the north-eastern and southern flanks of the volcano, and involved extensive lava emplacement, strombolian explosions, lava fountaining and phreato-magmatic activity (Christopher et al., 2001; Pompilio et al., 2001). Fig. 10 shows how gross variations in emitted radiance detected by MODVOLC depict a sharp initial rise to a peak between 20 and 22 July, followed by a decline in hot-spot radiance, a secondary peak between 27 and 29 July, and then a gradual decline until 7 August. The complex nature of the activity means that we cannot correlate these patterns unambiguously with, for example, lava eruption rates or the opening of new vents. The total radiance detected on any given day during this period will comprise that emitted by active lava flows of varying ages, lava-fountains, strombolian explosions, and also burning vegetation. Understanding day-to-day variations in detected radiance is further complicated due to an unknown and variable amount of signal attenuation due to fluctuations in the large amount of ash ejected during the eruption. However, available field reports

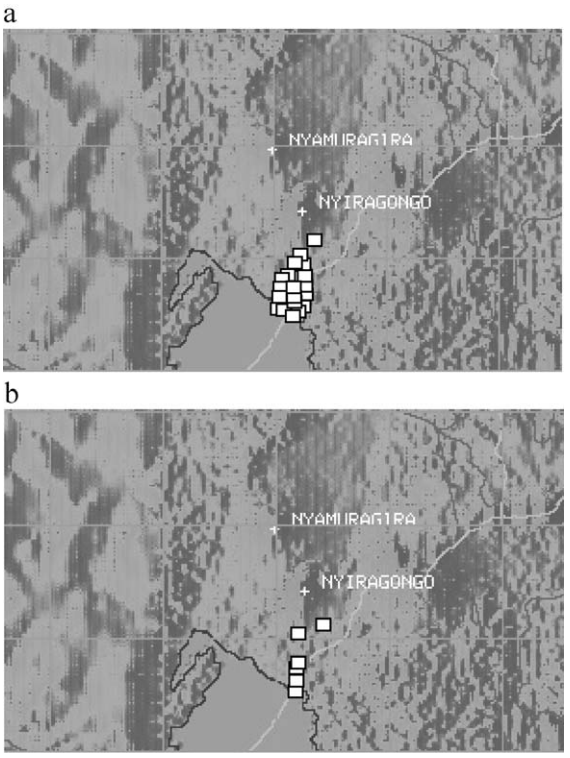

Fig. 9. Image maps taken from the HIGP MODVOLC web site showing lava flows detected at Nyiragongo on 18 January (a) and 21 January 2002 (b).

(GVN, 2001b) make reference to three main phases of the eruption which correlate with the MODVOLC radiance time-series; a primary peak in activity which occurred between 21 and 23 July, a secondary peak which occurred around 28 July, and a waning period which extended from 1 August to the 8 August, when the eruption ended.

This example highlights a significant limitation of the MODVOLC system. A substantial dip in detected 4-μm radiance occurs on 21 July relative to high levels recorded on 20 and 23 July. This could be the result of a short-term decrease in eruption intensity, although as field reports (GVN, 2001b) indicate that during this period as a whole eruption intensity was at its peak, this supposition is unlikely. A more likely explanation is that the lava flows, fire-fountains and vents active at this time were obscured by the substantial ash plumes produced during the peak phases of the eruption. However, without the original image data, or other extraneous information, the impact of volcanic ash (or meteorological clouds) on MODVOLC radiance time-series cannot be ascertained. Thus, caution must be exercised when interpreting variations in radiance detected by MODVOLC, as short-term oscillations could simply be an artefact of the prevailing weather conditions rather than real changes in eruptive activity. We note however that in this example, and others given by Wright et al. (2002a) and Flynn et al. (2002), general trends in MODVOLC detected radiances provide a faithful representation of how the eruptions in question have developed.

4.3. Lava domes

Silicic lava domes pose a different set of problems in terms of their remote detection than lava flows. They are usually smaller, erupted at slightly lower temperatures and at lower eruption rates. MODVOLC has detected the presence of active lava domes at a wide range of active volcanoes (Table 1; Fig. 11), although as we will see, detection can depend on emplacement style.

Since December 1994 activity at Popocatépetl has been characterised by three main processes; exhalations of gas and ash, explosions of lithic and juvenile material, and cycles of lava dome growth and destruction (Wright et al., 2002b). Fig. 12 shows the total amount of 4-μm radiance detected by MODVOLC at Popocatépetl for the period 1 June 2000

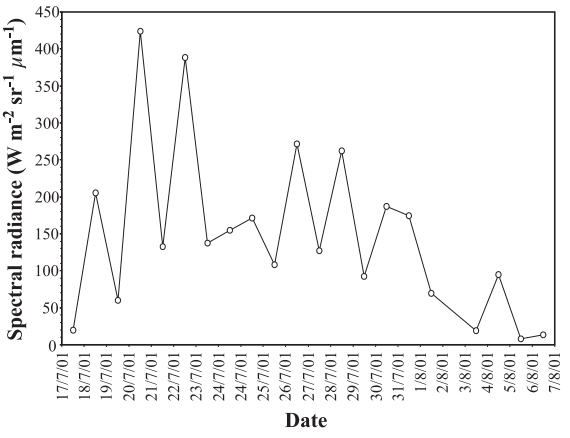

Fig. 10. The total amount of 4-μm spectral radiance detected by MODVOLC (i.e. summed for all pixels identified as hot spots by the algorithm) during the July–August 2001 flank eruption of Mount Etna.

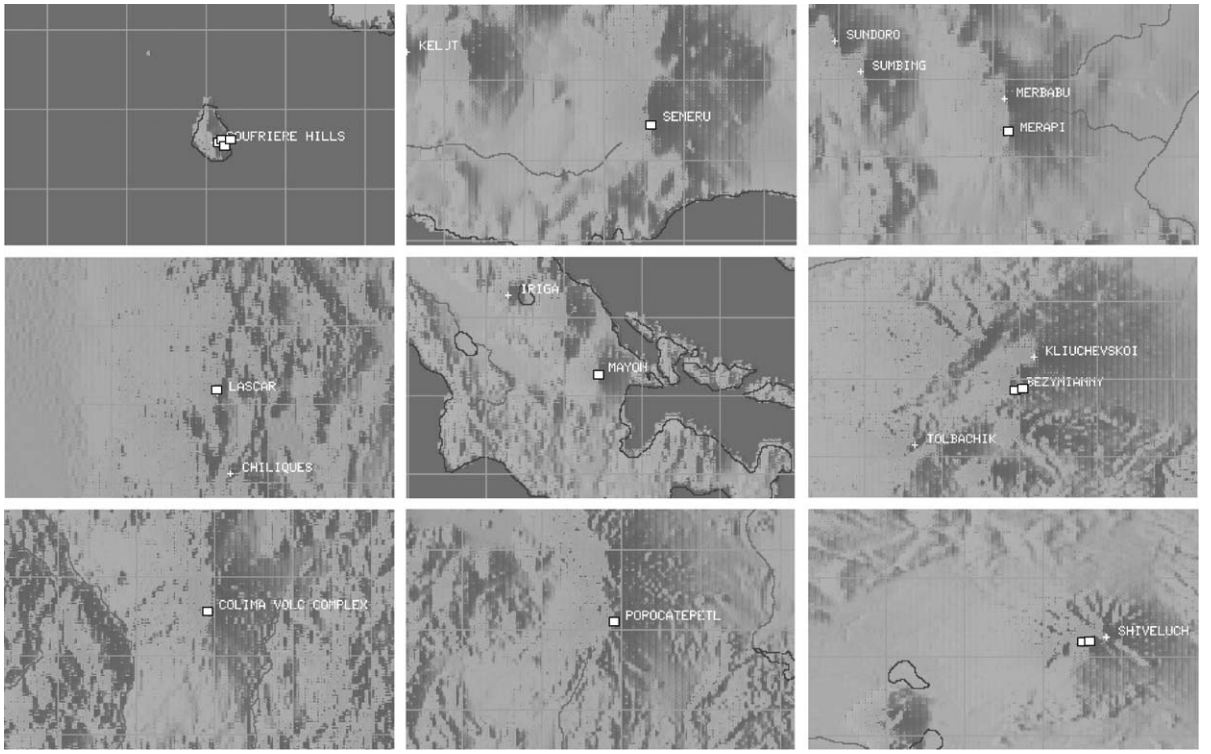

Fig. 11. Image maps taken from the HIGP MODVOLC web site showing lava domes detected at (top to bottom, left to right) Soufriere Hills, Montserrat (1 April 2002), Semeru, Java (23 May 2002), Merapi, Java (23 October 2001), Lascar, Chile (14 February 2001), Mayon, Philippines (20 July 2001), Bezymianny, Kamchatka (12 December 2001), Colima, México (16 February 2002), Popocatépetl, México (19 December 2001), and Shiveluch, Kamchatka (1 May 2002).

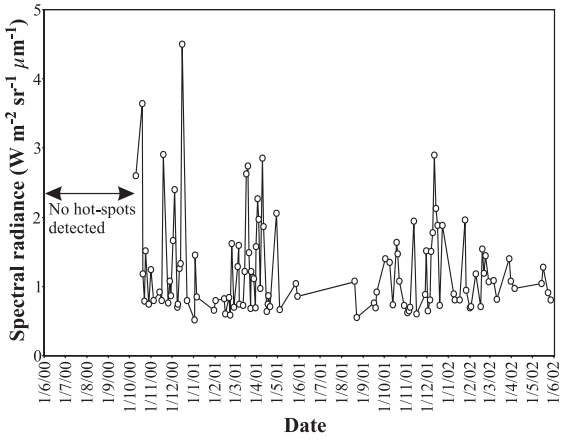

Fig. 12. The total amount of 4-μm spectral radiance detected by MODVOLC (i.e. summed for all pixels identified as hot spots by the algorithm) during the period 1 June 2000 to 1 June 2002 at Popocatépetl.

and 1 June 2002. Levels of activity between June and September 2000 were low, characterised only by low-intensity exhalations of gas and ash (GVN, 2000a) and MODVOLC detected no hot spots during this period. A new, very small lava dome was observed in the summit crater on 16 September 2000 (GVN, 2000b) and MODVOLC reports the first hot spot of this period on 10 October 2000. After this point, there is clear evidence for three periods of elevated radiative output; mid-November to late-December 2000, early-March to late-April 2001 and mid-November 2001 late-February 2002. Field reports (GVN, 2000c; GVN, 2001c; GVN, 2002a) confirm that each of these clusters (which interestingly, define a waxing and waning trend in radiant output) corresponds to an episode of lava dome growth and explosive destruction.

Although MODVOLC reliably documents each of these three phases of dome growth, the source of the

hot spots remains uncertain. Wright et al. (2002b) used 4-μm GOES data to perform a high-temporal resolution analysis of dome growth cycles at Popocatépetl during November and December 1998. They found that even though a lava dome occupied the summit crater throughout this entire period, elevated levels of radiance were apparent only on certain days. Analysis of real-time seismic amplitude and SO_2 gas flux data revealed that periods of high-thermal emission were correlated with explosions at the dome, which served to disrupt the cool dome carapace and expose the much hotter interior to the orbiting sensor. Thus, it was not the presence of the dome itself that produced elevated levels of radiance but rather transient processes affecting its surface temperature. Similar inferences can be made from other remote sensing studies of lava domes. Time-series of SWIR radiance emitted by the lava dome at Làscar (northern Chile) indicate that variations in high-temperature degassing were the main cause of variations in emitted SWIR radiance (Oppenheimer et al., 1993; Wooster and Rothery, 1997a) while Wooster and Kaneko (1998) found that variations in fumarolic heating of the lava dome formed during the 1992–1995 eruption at Unzen (Japan) could mask variations in dome area caused by increased eruption rates.

Consider this as we recount the performance of MODVOLC during the current dome growth episode at Colima volcano, western México. A small (~ 50-m diameter) dome was observed within Colima's summit crater on 26 May 2001, 25 months after the last phase of effusive activity (GVN, 2002b). However, it was not until the 16 February 2002 that MODVOLC reported the existence of a hot spot at the volcano (Fig. 13). It appears, however, that this hot spot was not a response to an increase in the level of activity (eruption rates had remained relatively constant at ~ 1 m^3 s^{-1} during December 2001 and January 2002; De La Cruz-Reyna, personal communication), but rather by a change in eruption style. On 14 February, the growing dome over-topped the crater walls and extended as a series of block lava flows down the flanks of the volcano, intermittent collapse of which produced incandescent avalanches and pyroclastic flows (GVN, 2002b). This transition in the mode of occurrence of the erupted lava, from a crater-confined dome to a series of spatially unconfined and collapsing block flows (which would enhance

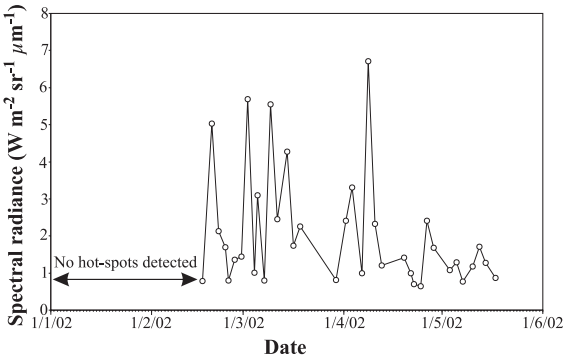

Fig. 13. The total amount of 4-μm spectral radiance detected by MODVOLC (i.e. summed for all pixels identified as hot spots by the algorithm) during the period 1 January to 1 June 2002 at Colima volcano.

the exposure of hotter material from the lava core) seems to have triggered the detection of hot spots by MODVOLC. Since this time MODVOLC has detected hot-spots at Colima on a further 36 occasions at frequent intervals (Fig. 13), consistent with the nature of the ongoing activity, whereby block lava flows continue to extend down the upper flanks of the volcano, occasionally collapsing to form pyroclastic flows (GVN, 2002b).

The influence of eruptive style on the radiance emitted by a lava dome is further illustrated with reference to recent and ongoing eruption at Shiveluch, Kamchatka. MODVOLC reported a hot spot on 30 April 2001, 2 weeks before the new dome was first observed on 12 May 2001. As of 1 January 2003, MODVOLC reported hot spots at Shiveluch on a near daily basis (Fig. 14a). This is consistent with the style of volcanism that persisted during this period, whereby frequent explosions and gravitational collapse of the dome generate extensive pyroclastic flows (GVN, 2002c) regularly exposing hot material from the dome interior. A similar situation persists at Soufriere Hills volcano, Montserrat, where frequent collapse of a growing and unstable dome over a prolonged period (GVN, 2001d,e, 2002d) has resulted in regular detection of hot spots by MODVOLC (Fig. 14b).

It appears that prior to a change in eruption style, the Colima dome, perhaps because it was emplaced largely aseismically and possibly also endogenously (GVN, 2001f), simply did not emit enough SWIR radiance to trip the MODVOLC alert threshold. The

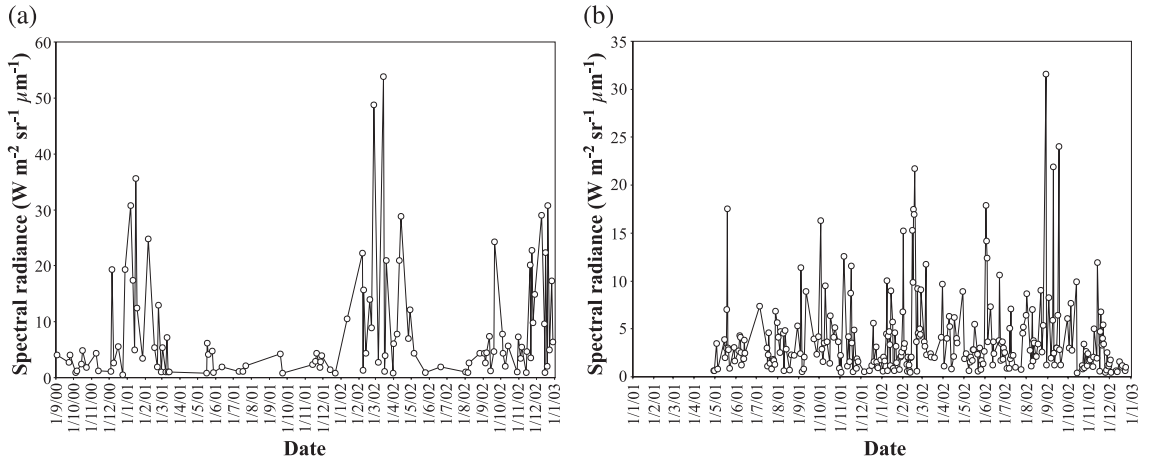

Fig. 14. The total amount of 4-μm spectral radiance detected by MODVOLC (i.e. summed for all pixels identified as hot spots by the algorithm at Soufriere Hills volcano [Montserrat; (a)] and Shiveluch [Kamchatka; (b)] for the period 1 September 2000 to 31 December 2002 and 1 January 2001 to 31 December 2002, respectively.

same may also be true for Láscar volcano (Chile) where despite the presence of a lava dome, MODVOLC has reported only five hot spots throughout the 573-day monitoring period we report here. These examples indicate that MODVOLC can fail to identify the initial emplacement or passive presence of a lava dome, depending on how the lava is erupted. However, they also show that processes associated with increasing levels of activity such as explosions and dome collapse will generate the kind of hot spots that MODVOLC detects on a regular basis.

4.4. Vent-dominated activity

The automated detection of sporadic, vent-based activity is a complex function of sampling frequency, event frequency, event magnitude, event duration and the time for which the evidence of such a thermal event can be expected to persist in the SWIR radiance record. For example, whether a strombolian eruption produces a detectable thermal anomaly depends on how much material is ejected during the explosion and how recently the explosion occurred prior to satellite overpass (Dehn et al., 2000). Furthermore, given that the sampling frequency of orbiting satellites is fixed, the lower the frequency of such explosions, the lower the probability that evidence of such events is preserved in the spectral radiance record.

Although episodes of increased seismicity had occurred at Karymsky (Kamchatka) since September 2000, early January 2002 saw a significant increase in the number of shallow events affecting the volcano (GVN, 2002e). Both MODVOLC and the Kamchatkan Volcanic Eruption Response Team (KVERT, via analysis of AVHRR data; GVN, 2002e) report the appearance of a hot spot at Karymsky on 19 January

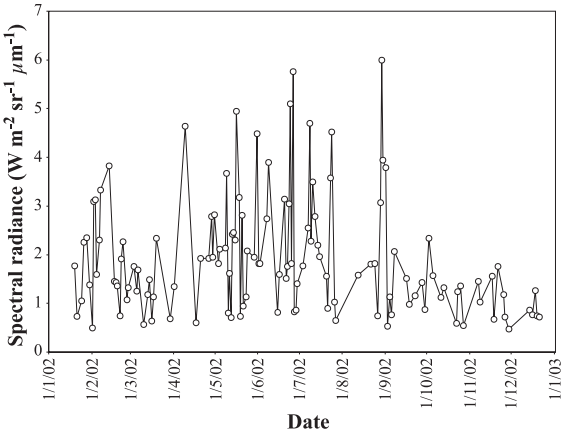

Fig. 15. The total amount of 4-μm spectral radiance detected by MODVOLC (i.e. summed for all pixels identified as hot spots by the algorithm) during the period 1 November 2002 to 28 February 2003 at Karymsky (Kamchatka) for the period 1 January 2002 to 31 December 2002.

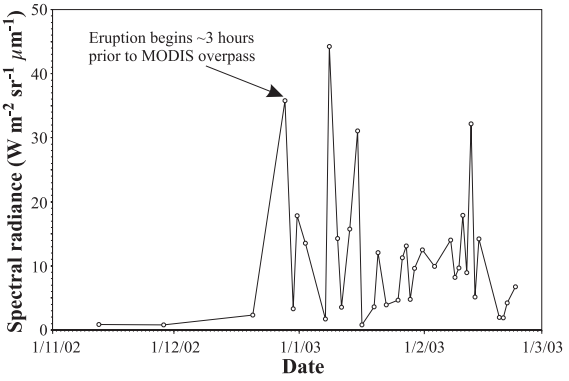

Fig. 16. The total amount of 4-μm spectral radiance detected by MODVOLC (i.e. summed for all pixels identified as hot spots by the algorithm) during the period 1 November 2002 to 28 February 2003 at Stromboli volcano.

2002. Since then MODVOLC has reported hot spots on a frequent basis (Fig. 15), probably associated with strombolian activity characteristic of this volcano.

The situation is, however, quite different at Stromboli volcano, Italy. Despite the fact that Stromboli is known to have produced mild stromblian explosions at a rate of approximately 10 per hour for at least the last 2000 years (Rosi et al., 2000). MODVOLC only detected two hot spots in 19 months up to June 2002. Given that the frequency of explosions at Stromboli is similar to that at Karymsky, the only explanation for this is that the thermal anomalies (e.g. ejecta blankets, ambient vent surface temperatures) produced by explosions at Stromboli are insufficient to trip the MODVOLC alert threshold. Hot spots have been frequently observed since December 2002, however, due to the recent episode of lava effusion (Fig. 16).

5. Limitations of MODVOLC and interpretation of the data

MODVOLC was intended to provide rapid access to information regarding the global distribution of hot spots by running at an early stage of the MODIS data processing chain with no data dependencies (Kaufman et al., 1998). This is reflected in the operational constraints under which the algorithm was developed. However, the necessary simplicity of MODVOLC has resulted in certain limitations that must be addressed here.

The need to set detection thresholds is common to all thermal monitoring systems. All such systems face the same dilemma: setting thresholds too high results in failure to detect a certain number of real hot spots; setting them too low results in false alarms and promotes a lack of trust in the results. Inspection of the MODIS Big Island image shown in Fig. 3c reveals up to 21 pixels that appear, visually, to be 'bright', and hence, thermally anomalous. However, only 13 of these were automatically classified as hot spots by MODVOLC. The implications of this will vary with context. MODVOLC is intended to facilitate rapid detection of hot spots and should not to be thought of as to be an all-encompassing thermal analysis tool. As such, by detecting 13 of the 21 anomalous pixels portrayed in Fig. 3c, the algorithm has fulfilled its role. The same cannot be said for a volcano that is characterised solely by low levels of activity if the amount of radiance emitted is insufficient to trip the MODVOLC threshold, as such activity will go unreported by the algorithm. The problem of setting thresholds is a trait common to all automated hot-spot monitoring systems and it is impossible to automatically detect all of the thermal anomalies all of the time while eliminating all 'false-positives'. However, we hope the examples recounted herein and by Wright et al. (2002a) and Flynn et al. (2002) illustrate that MODVOLC provides a reliable means of hot-spot detection for a wide range of eruptive styles and intensities.

The fact that MODVOLC returns no image data can lead to ambiguity when interpreting radiance time-series at individual volcanoes, as the influence that clouds and eruption plumes have on the detection process cannot be quantified. For this reason, short-term (i.e. day-to-day) variations in the intensity of hot spots reported by MODVOLC may not be directly related to variations in the level of volcanic activity. However, the examples we present in the previous sections indicate that gross trends in emitted SWIR radiance appear to faithfully represent general changes in the level of activity. Establishing the general radiative behaviour of a volcano using standard statistical measures (e.g. Wright et al., 2002b) is eminently achievable given the long (and therefore temporally representative time-series) for radiance data that MODVOLC provides.

MODVOLC does not discriminate between different high-temperature sources but, as illustrated in

Section 4.1, the excellent geolocation of MODIS image pixels means hot spots can be confidently attributed to known centres of volcanic activity. Confusion could arise, however, on volcanoes whose summit regions are heavily vegetated if ejection of high-temperature material ignited this vegetation. Similarly, the radiance emitted by fires started by encroachment of lava flows into vegetated areas would be impossible to isolate from the volcanic radiance signal.

Implementation of MODVOLC was initially hampered by data processing bottlenecks at the GSFC DAAC (Flynn et al., 2002), and as a result several data gaps exist in our hot-spot archive. This situation has improved substantially however and the time lag between acquisition of the raw MODIS data and internet posting of the hot-spot results has fallen to less than 24 h. Thus, although the system will never provide real-time data regarding the thermal status of the Earth's active volcanoes, a situation of near-real-time operation has been achieved.

6. Conclusions

MODVOLC was intended to provide rapid access to information regarding the global distribution of hot spots. As such, MODVOLC is not the most sophisticated hot-spot monitoring system in operation or indeed the most sophisticated that could be designed. However, the examples we present show that the system reliably detects hot spots associated with a wide range of eruptive styles and it does this, uniquely, at a global scale. The routine monitoring of global volcanism is important for monitoring remote volcanoes as well as those which are otherwise poorly instrumented. This is exemplified by the role played by MODVOLC in the discovery of active volcanism at Mount Belinda on Montagu Island in the South Sandwich islands, a volcano with no previous record of Holocene activity. The algorithm also recorded the period during November 2002 when Kavachi, a submarine volcano in the Solomon Islands, briefly made an appearance above sea level. By designing the algorithm to eliminate erroneous hot-spot detection, we realise that we forgo the detection of low-intensity thermal anomalies, but find this preferential to a situation where the results of the algorithm cannot be trusted.

Although this paper deals solely with the nighttime version of the MODVOLC algorithm, a provisional version of a daytime algorithm has recently been implemented and is currently being evaluated. When fully operational, it will allow two hot-spot observations per day for most areas of the Earth. The sampling frequency of MODVOLC will be improved still further when data from a second MODIS sensor recently launched on the EOS Aqua satellite, is incorporated into the system. As Terra and Aqua have different descending-node equatorial crossing times (10:30 AM and 2:30 PM respectively), synergy of the data provided by both MODIS sensors will allow four hot-spot observations per day (morning, afternoon, evening and night). This has implications for monitoring dynamic volcanic phenomenon such as active lava flows, as well as for ameliorating the detrimental effect that cloud cover can have on constructing detailed radiance time-series. When fully operational, we anticipate that MODVOLC will provide an integrated resource for detecting, archiving and disseminating information regarding the global occurrence of volcanic eruptions.

Acknowledgements

Funded by NASA Pathfinder grant NAG5-9413. RW acknowledges a conference travel grant from The Royal Society of London, which funded attendance of the 2001 AGU Fall Meeting, from which this special volume stems. HIGP publication number 1321 and SOEST publication number 6347.

References

Christopher, T.E., Pyle, D.M., Burton, M.R., Oppenheimer, C.M., 2001. Eruptive products and processes: Mt Etna, Sicily, 2001. EOS, Transactions-American Geophysical Union 82 (47), Fall Meet. Suppl., Abstract, V42A-0991.

Dehn, J., Dean, K., Engle, K., 2000. Thermal monitoring of North Pacific volcanoes from space. Geology 28, 755–758.

Donegan, S., Flynn, L.P., 2004. Comparison of the response of the Landsat 7 enhanced Thematic Mapper plus and the Earth Observing-1 advanced land imager over active lava flows. Journal of Volcanology and Geothermal Research 135, 105–126 (this issue).

Flasse, S.P., Ceccato, P.S., 1996. A contextual algorithm for AVHRR fire detection. International Journal of Remote Sensing 17, 419–424.

Flynn, L.P., Mouginis-Mark, P.J., Horton, K.A., 1994. Distribution of thermal areas on an active lava flow field: Landsat observations of Kilauea, Hawaii, July 1991. Bulletin of Volcanology 56, 284–296.

Flynn, L.P., Wright, R., Garbeil, H., Harris, A.J.L., Pilger, E., 2002. A global thermal alert using MODIS: initial results from 2000–2001. Advances in Environmental Monitoring and Modeling 1, 37–69.

Francis, P.W., McAllister, R., 1986. Volcanology from space; using Landsat Thematic Mapper data in the Central Andes. EOS, Transactions-American Geophysical Union 67, 170–171.

Francis, P.W., Rothery, D.A., 1987. Using the Landsat Thematic Mapper to detect and monitor active volcanoes: an example from Lascar volcano, Northern Chile. Geology 15, 614–617.

Gawarecki, S.J., Lyon, R.J.P., Nordberg, W., 1965. Infrared spectral returns and imagery of the Earth from space and their application to geological problems: scientific experiments for manned orbital flight. American Astronautical Society, Science and Technology Series 4, 13–133.

GVN, W., 2000a. Popocatépetl. Bulletin of the Global Volcanism Network 25 (7), 14.

GVN, W., 2000b. Popocatépetl. Bulletin of the Global Volcanism Network 25 (10), 3.

GVN, W., 2000c. Popocatépetl. Bulletin of the Global Volcanism Network 25 (12), 2–5.

GVN, W., 2001a. Nyiragongo. Bulletin of the Global Volcanism Network 26 (12), 2–5.

GVN, W., 2001b. Etna. Bulletin of the Global Volcanism Network 26 (9), 2–5.

GVN, W., 2001c. Popocatépetl. Bulletin of the Global Volcanism Network 26 (8), 11–14.

GVN, W., 2001d. Soufriere hills. Bulletin of the Global Volcanism Network 26 (2), 7–9.

GVN, W., 2001e. Soufriere hills. Bulletin of the Global Volcanism Network 26 (7), 6–7.

GVN, W., 2001f. Colima. Bulletin of the Global Volcanism Network 26 (5), 11–13.

GVN, W., 2002a. Popocatépetl. Bulletin of the Global Volcanism Network 27 (2), 6–8.

GVN, W., 2002b. Colima. Bulletin of the Global Volcanism Network 27 (2), 6–8.

GVN, W., 2002c. Shiveluch. Bulletin of the Global Volcanism Network 27 (3), 6–8.

GVN, W., 2002d. Soufriere hills. Bulletin of the Global Volcanism Network 27 (4), 6–8.

GVN, W., 2002e. Karymsky. Bulletin of the Global Volcanism Network 27 (3), 6–8.

Harris, A.J.L., Stevenson, D.S., 1997. Thermal observations of open degassing conduits and fumaroles at Stromboli and Vulcano using remotely sensed data. Journal of Volcanology and Geothermal Research 76, 175–198.

Harris, A.J.L., Blake, S., Rothery, D.A., Stevens, N.F., 1997a. A chronology of the 1991 to 1993 Etna eruption using advanced very high resolution radiometer data: implications for real-time thermal volcano monitoring. Journal of Geophysical Research 102, 7985–8003.

Harris, A.J.L., Butterworth, A.L., Carlton, R.W., Downey, I., Miller, P., Navarro, P., Rothery, D.A., 1997b. Low-cost volcano surveillance from space: case studies from Etna, Krafla, Cerro Negro, Fogo, Lascar and Erebus. Bulletin of Volcanology 59, 49–64.

Harris, A.J.L., Keszthelyi, L., Flynn, L.P., Mouginis-Mark, P.J., Thornber, C., Kauahikaua, J., Sherrod, D., Trusdell, F., Sawyer, M.W., Flament, P., 1997c. Chronology of the episode 54 eruption at Kilauea volcano, Hawaii, from GOES-9 satellite data. Geophysical Research Letters 24, 3281–3284.

Harris, A.J.L., Flynn, L.P., Rothery, D.A., Oppenheimer, C., Sherman, S.B., 1999. Mass flux measurements at active lava lakes: implications for magma recycling. Journal of Geophysical Research 104, 7117–7136.

Harris, A.J.L., Pilger, E., Flynn, L.P., Garbeil, H., Mouginis-Mark, P.J., Kauahikaua, J., Thornber, C., 2001. Automated, high temporal resolution, thermal analysis of Kilauea volcano, Hawaii, using GOES satellite data. International Journal of Remote Sensing 22, 945–967.

Justice, C.O., Giglio, L., Korontzi, S., Owens, J., Morisette, J.T., Roy, D., Descloitres, J., Alleaume, S., Petitcolin, F., Kaufman, Y., 2002. The MODIS fire products. Remote Sensing of Environment 83, 244–262.

Kaneko, T., Wooster, M.J., 1999. Landsat infrared analysis of fumarole activity at Unzen volcano: time-series comparison with gas and magma fluxes. Journal of Volcanology and Geothermal Research 89, 57–64.

Kaneko, T., Yasuda, A., Ishimaru, T., Takagi, M., Wooster, M.J., Kagiyama, T., 2002a. Satellite monitoring of Japanese volcanoes: a prototype AVHRR-based system. Advances in Environmental Monitoring and Modelling 1, 125–133.

Kaneko, T., Wooster, M.J., Nakada, S., 2002b. Exogenous and endogenous growth of the Unzen lava dome examined by satellite infrared image analysis. Journal of Volcanology and Geothermal Research 116, 151–160.

Kaufman, Y.J., Justice, C.O., Flynn, L.P., Kendall, J.D., Prins, E.M., Giglio, L., Ward, D.E., Menzel, W.P., Setzer, A.W., 1998. Potential global fire monitoring from EOS-MODIS. Journal of Geophysical Research 103, 32215–32238.

Kilburn, C.R.J., Pinkerton, H., Wilson, L., 1995. Forecasting the behaviour of lava flows. In: McGuire, B., Kilburn, C.R.J., Murray, J.B. (Eds.), Monitoring Active Volcanoes. UCL Press, London, pp. 346–368.

Oppenheimer, C., 1991. Lava flow cooling estimated from Landsat Thematic Mapper infrared data: the Lonquimay eruption (Chile, 1989). Journal of Geophysical Research 96, 21865–21878.

Oppenheimer, C., 1998. Volcanological applications of meteorological satellites. International Journal of Remote Sensing 19, 2829–2864.

Oppenheimer, C., Francis, P.W., 1997. Remote sensing of heat, lava and fumarole emissions from Erta 'Ale volcano, Ethiopia. International Journal of Remote Sensing 18, 1661–1692.

Oppenheimer, C., Francis, P.W., Rothery, D.A., Carlton, R.W.T., Glaze, L.S., 1993. Infrared image analysis of volcanic thermal features: Lascar volcano, Chile, 1984–1992. Journal of Geophysical Research 98, 4269–4286.

Pompilio, M., Corsaro, R., Freda, C.A.F., Miraglia, L.A.F.,

Scarlato, P.A.F., Gomez-Palacios, J.J., Taddeucci, J., 2001. Petrological evidences of a complex plumbing system feeding the July–August 2001 eruption of Mt. Etna. EOS Transaction-American Geophysical Union 82 (7), Fall Meet. Suppl., Abstract, V52C-08.

Prins, E.M., Menzel, W.P., 1992. Geostationary satellite detection of biomass burning in South America. International Journal of Remote Sensing 13, 2783–2799.

Prins, E.M., Menzel, W.P., 1994. Trends in South American biomass burning detected with the GOES visible infrared spin scan radiometer atmospheric sounder from 1983 to 1991. Journal of Geophysical Research 99, 16719–16735.

Rosi, M., Bertagnini, A., Landi, P., 2000. Onset of the persistent activity at Stromboli volcano (Italy). Bulletin of Volcanology 62, 294–300.

Rothery, D.A., Francis, P.W., Wood, C.A., 1988. Volcano monitoring using short wavelength infrared data from satellites. Journal of Geophysical Research 93, 7993–8008.

Rothery, D.A., Oppenhemier, C., Bonneville, A., 1995. Infrared thermal monitoring. In: McGuire, B., Kilburn, C.R.J., Murray, J.B. (Eds.), Monitoring Active Volcanoes. UCL Press, London, pp. 184–216.

Rothery, D.A., Thorne, M.T., Flynn, L.P., 2003. MODIS thermal alerts in Britain and the North Sea during the first half of 2001. International Journal of Remote Sensing 24, 817–826.

Schneider, D.J., Dean, K.G., Dehn, J., Miller, T.P., Kirianov, V.U., 2000. Monitoring and analyses of volcanic activity using remote sensing data at the Alaska volcano observatory: case study for Kamchatka, Russia, December 1997. In: Mouginis-Mark, P.J., Crisp, J.A., Fink, J.H. (Eds.), Remote Sensing of Active Volcanism. American Geophysical Union Monograph, vol. 116, pp. 65–85. Washington, DC.

Scorer, R.S., 1986. Etna: the eruption of Christmas 1985 as seen by a meteorological satellite. Weather 41, 378–384.

Simkin, T., Siebert, L., 1994. Volcanoes of the World, 2nd ed. Geoscience Press, Tuscon, 368 pp.

Weisnet, D.R., D'Aguanno, J., 1982. Thermal imagery of Mount Erebus from the NOAA-6 satellite. Antarctic Journal of the United States 17, 32–34.

Williams, R.S., Friedman, J.D., 1970. Satellite observation of effusive volcanism. Journal of the British Interplanetary Society 23, 441–450.

Wooster, M.J., Rothery, D.A., 1997a. Thermal monitoring of Lascar volcano, Chile, using infrared data from the along-track scanning radiometer: a 1992–1995 time series. Bulletin of Volcanology 58, 566–579.

Wooster, M.J., Rothery, D.A., 1997b. Time series analysis of effusive volcanic activity using the ERS along track scanning radiometer: the 1995 eruption of Fernandina volcano, Galapagos Islands. Remote Sensing of Environment 62, 109–117.

Wooster, M.J., Kaneko, T., 1998. Satellite thermal analyses of lava dome effusion rates at Unzen volcano, Japan. Journal of Geophysical Research 103, 20935–20947.

Wright, R., Flynn, L.P., Harris, A.J.L., 2001. Evolution of lava flow-fields at Mount Etna, 27–28 October 1999, observed by Landsat 7 ETM+. Bulletin of Volcanology 63, 1–7.

Wright, R., Flynn, L., Garbeil, H., Harris, A., Pilger, E., 2002a. Automated volcanic eruption detection using MODIS. Remote Sensing of Environment 82, 135–155.

Wright, R., De La Cruz-Reyna, S., Flynn, L.P., Harris, A.J.L., Gomez-Palacios, J.J., 2002b. Infrared satellite monitoring of Popocatépetl: explosions, exhalations and cycles of dome growth. Journal of Geophysical Research 107 (B8), 2153 (doi: 10.1029/2000JB000125).